INTERNATIONAL JOURNAL FOR NUMERICAL METHODS IN FLUIDS
Int. J. Numer. Meth. Fluids 2006; **50**:377–396
Published online 31 October 2005 in Wiley InterScience (www.interscience.wiley.com). DOI: 10.1002/fld.1111

Finite analytic boundary condition for a higher-order finite analytic scheme

S. H. Lee[1,*,†] and B. K. Soni[2,‡]

[1]*Hydrodynamic Research Department, Hyundai Heavy Industries Co. Ltd, South Korea*
[2]*Mechanical Engineering, University of Alabama at Birmingham, U.S.A.*

SUMMARY

A higher-order finite analytic scheme based on one-dimensional finite analytic solutions is used to discretize three-dimensional equations governing turbulent incompressible free surface flow. In order to preserve the accuracy of the numerical scheme, a new, finite analytic boundary condition is proposed for an accurate numerical solution of the partial differential equation. This condition has higher-order accuracy. Thus, the same order of accuracy is used for the boundary. Boundary conditions were formulated and derived for fluid inflow, outflow, impermeable surfaces and symmetry planes. The derived boundary conditions are treated implicitly and updated with the solution of the problem. The basic idea for the derivation of boundary conditions was to use the discretized form of the governing equations for the fluid flow simplified on the boundaries and flow information. To illustrate the influence of the higher-order effects at the boundaries, another, lower-order finite analytic boundary condition, is suggested. The simulations are performed to demonstrate the validity of the present scheme and boundary conditions for a Wigley hull advancing in calm water. Copyright © 2005 John Wiley & Sons, Ltd.

KEY WORDS: boundary condition; higher-order finite analytic scheme; free surface flow

1. INTRODUCTION

Numerical methods that have been generally used to discretize partial differential equations are finite volume, finite difference, and finite element methods. Another method used to discretize partial differential equations is the finite analytic method. In this method, the equations are discretized by analytic methods. The finite analytic method avoids the truncation error and spurious oscillations produced in the approximation of the differential equation. Compared to the finite volume method, the finite analytic method has some advantages. One of these advantages is the implicit treatment of the terms in the second derivative. Another major advantage is

*Correspondence to: S. H. Lee, Hydrodynamic Research Department, Hyundai Heavy Industries Co. Ltd, 1, Chunha-Dong, Dong-Gu, Ulsan 682-060, South Korea.
†E-mail: slee@hhi.co.kr
‡E-mail: bsoni@uab.edu

Received 6 April 2005
Revised 12 September 2005
Accepted 12 September 2005

that it provides an automatic upwind shift depending on local cell Reynolds number. In order to discretize three-dimensional elliptic partial differential equations (PDEs) analytically, a 27-point finite analytic scheme was first derived [1]. The scheme is based on a three-dimensional analytic solution to a three-dimensional viscous flow field. Then, 12-point and 19-point finite analytical schemes were introduced [2, 3]. The 12-point finite analytic scheme was derived using one- and two-dimensional analytic solutions. The 19-point scheme was derived using the superposition of the local analytic solutions of the linearized two-dimensional equations. An 8-point finite analytic scheme was also derived using a one-dimensional analytic solution [4]. The schemes in the finite analytic method have a width of three mesh points in each coordinate direction. The schemes previously used in the finite analytic method have been applied only to elliptic PDEs. In the present research, higher order schemes were derived and applied to three-dimensional elliptic and hyperbolic PDEs. The values on the cell faces were interpolated using local analytic solutions having a width of four nodal points. The scheme had a width of five mesh points in each coordinate direction.

There have been many researches about free surface flow around a ship hull [5–13]. In considering free surface flow, wave reflections at the open boundaries may degrade the accuracy of the solution. Achieving far field predictions of sufficient accuracy for a ship hull is still a difficult task. In order to prevent the reflected waves from spreading, more accurate boundary conditions may be added at the boundaries of the finite computational domain [14–19]. Neumann and Dirichlet boundary conditions have been widely used in the field of ship hydrodynamics. In the present study, finite analytic boundary conditions were developed and applied to incompressible free surface flow problems. Finite analytic boundary conditions can be applied to both elliptic and hyperbolic PDEs. The main purpose of this study is to derive three-dimensional higher-order finite analytic scheme and boundary conditions.

2. GOVERNING EQUATIONS OF FLUID FLOW

The vector form of incompressible Reynolds-averaged Navier–Stokes (RANS) equations, the kinematic boundary conditions, and the pressure Poisson equation are given for a free surface flow problem as

$$\frac{\partial \underline{u}}{\partial t} + (\nabla \underline{u}) \cdot \underline{u} = -\nabla P + v_E \nabla^2 \underline{u} + [\nabla \underline{u} + (\nabla \underline{u})^{\mathrm{T}}] \cdot \nabla v_E \tag{1}$$

where

$$P = p + \frac{z}{Fn^2} + \frac{2}{3}k \quad \text{and} \quad v_E = \frac{1}{R_{\text{eff}}} = \frac{1}{Re} + v_t$$

$$\frac{\partial F}{\partial t} + \underline{u} \cdot \nabla F = 0 \tag{2}$$

$$\nabla^2 P = \frac{(\nabla \cdot \underline{u})^n}{\triangle \tau} - (\nabla \underline{u})^{\mathrm{T}} : \nabla \underline{v} + \nabla^2 \underline{u} \cdot \nabla v_E + [\nabla \underline{u} + (\nabla \underline{u})^{\mathrm{T}}] : \nabla(\nabla v_E) \tag{3}$$

The above equations are dimensionless. In Equation (1), Fn is a Froude number used to normalize the gravity constant, p is a static pressure and k is a turbulent kinetic energy. v_t and R_{eff} represent the eddy viscosity and the effective Reynolds number, respectively. In Equation (2), F is the equation of the surface. Equation (2) represents the kinematic boundary condition and is used to update the unknown free surface location. The concept of the material surface is used for the free surface. We assume that the flow particles on the upper boundary move up and down vertically. Thus, Equation (2) can be rewritten by substituting z-coordinate and $G(x, y, t)$ for the surface, F. In Equation (3), the pressure Poisson equation is derived by taking the divergence of Equation (1) and used to solve the velocity–pressure coupling problem. Viscous terms and viscosity-related terms are all included in the right-hand side of Equation (3). When the first-order backward scheme is used for the time derivative term, the continuity equation at time step $n+1$ is set to zero, while at time step n it is retained to eliminate the accumulation of numerical errors [19]. The continuity equation is satisfied indirectly through the solution of the pressure Poisson equation. The physical curvilinear component form of RANS equations, the kinematic boundary condition and the pressure Poisson equation are expressed as [20]

$$R_{\text{eff}} \frac{\partial u^{(i)}}{\partial \tau} + R_{\text{eff}} v^{(j)} u^{(i)}_{,(j)} = -R_{\text{eff}} g^{(ij)} \frac{\partial P}{\partial \xi^{(j)}} + g^{(jk)} \left[u^{(m)}_{,(j)} \Gamma^{(i)}_{(mk)} - u^{(i)}_{,(m)} \Gamma^{(m)}_{(jk)} + \frac{\partial u^{(i)}_{,(j)}}{\partial \xi^{(k)}} \right]$$

$$+ R_{\text{eff}} \frac{\partial v_E}{\partial \xi^{(j)}} [g^{(jk)} u^{(i)}_{,(k)} + g^{(ik)} u^{(j)}_{,(k)} \tag{4}$$

where

$$u^{(i)}_{,(k)} = \frac{\partial u^{(k)}}{\partial \xi^{(i)}} + u^{(m)} \Gamma^{(k)}_{(im)} \quad \text{and} \quad \Gamma^{(k)}_{(ij)} = \frac{\sqrt{g_{kk}}}{\sqrt{g_{ii}}\sqrt{g_{jj}}} \Gamma^{k}_{ij} - \delta_{i^k} \frac{g_{km}}{g_{ii}\sqrt{g_{jj}}} \Gamma^{m}_{ij}$$

$$\frac{\partial G}{\partial t} + u^{(1)} \frac{\partial G}{\partial \xi^{(1)}} + u^{(2)} \frac{\partial G}{\partial \xi^{(2)}} = w \tag{5}$$

$$\frac{\partial^2 P}{\partial \xi^{(k)} \xi^{(i)}} g^{(ik)} - g^{(jk)} \Gamma^{(i)}_{(jk)} \frac{\partial P}{\partial \xi^{(i)}}$$

$$= \frac{[u^{(i)}_{,(i)}]^n}{\triangle \tau} - u^{(k)}_{,(i)} u^{(i)}_{,(k)} + g^{(jk)} \left[u^{(m)}_{,(j)} \Gamma^{(i)}_{(mk)} - u^{(i)}_{,(m)} \Gamma^{(m)}_{(jk)} + \frac{\partial u^{(i)}_{,(j)}}{\partial \xi^{(k)}} \right] \frac{\partial v_E}{\partial \xi^{(i)}} + g^{(iq)} u^{(p)}_{,(j)} \frac{\partial^2 v_E}{\partial \xi^{(k)} \xi^{(i)}}$$

$$- g^{(iq)} \Gamma^{(j)}_{(ki)} u^{(k)}_{,(q)} \frac{\partial v_E}{\partial \xi^{(j)}} + g^{(qj)} u^{(i)}_{,(q)} \frac{\partial^2 v_E}{\partial \xi^{(k)} \xi^{(i)}} - g^{(qk)} \Gamma^{(j)}_{(ki)} u^{(i)}_{,(q)} \frac{\partial v_E}{\partial \xi^{(j)}} \tag{6}$$

The vector forms of the partial differential equations, in Equations (1)–(3) were transformed into the physical curvilinear component form. The full details of the derivation have been previously described [20]. The repeated indices imply a sum. Here, x_k are Cartesian

coordinates, ξ^i are curvilinear coordinates and $\xi^{(i)}$ are physical curvilinear coordinates. The relationship between the two coordinate systems, ξ^i and $\xi^{(i)}$, is defined as

$$\xi^{(i)} = \xi^{(i)}(\xi^i) \quad \text{where } \Delta\xi^{(i)} = \sqrt{g_{ii}}\Delta\xi^i \quad \text{and} \quad g_{ii} = \frac{\partial x_j}{\partial \xi^i}\frac{\partial x_j}{\partial \xi^i} \tag{7}$$

The following relationships are used in Equations (4)–(6) as

$$g_{(ij)} = \frac{1}{\sqrt{g_{ii}}}\frac{1}{\sqrt{g_{jj}}}g_{ij} \quad \text{where } g_{ij} = \frac{\partial x_k}{\partial \xi^i}\frac{\partial x_k}{\partial \xi^j} \tag{8}$$

$$g^{(ij)} = \sqrt{g_{ii}}\sqrt{g_{jj}}g^{ij} \quad \text{where } g^{ij} = \frac{\partial \xi^i}{\partial x_k}\frac{\partial \xi^j}{\partial x_k} \tag{9}$$

Components of the velocity vector, $u^{(i)}$, are defined as

$$u^{(i)} = \underline{u} \cdot \underline{a}_{(i)} \tag{10}$$

Here, the components of the velocity vector in Equation (10) have the same direction as that of the coordinate line and have meaningful physical values. The vector $\mathrm{d}\underline{r}$ can be used to show the relationship between two different covariant base vectors as

$$\mathrm{d}\underline{r} = \underline{a}_i\,\mathrm{d}\xi^i = \underline{a}_{(i)}\,\mathrm{d}\xi^{(i)} \quad \text{where } \underline{a}_i = \frac{\partial \underline{r}}{\partial \xi^i} \quad \text{and} \quad \underline{a}_{(i)} = \frac{\partial \underline{r}}{\partial \xi^{(i)}} \tag{11}$$

The relationship between two different velocity components is defined as

$$u^{(j)} = u(i)\sqrt{g_{jj}}\frac{\partial \xi^j}{\partial x_i} \quad (\text{sum on } i) \quad \text{and} \quad u(k) = \frac{1}{\sqrt{g_{jj}}}\frac{\partial x_k}{\partial \xi^j} \quad (\text{sum on } j) \tag{12}$$

The velocity components $u(i)$ in Equation (12) represent (u, v, w). The term $u^{(k)}_{(i)}$ in Equation (1) represent the covariant derivative of the contravariant physical velocity components and is defined as

$$u^{(k)}_{(i)} = u^{(j)}\Gamma^{(k)}_{(ji)} + \frac{\partial u^{(k)}}{\partial \xi^i} \tag{13}$$

$\Gamma^{(k)}_{(ij)}$ are regarded as physical counterparts of the Christoffel symbols and are defined as

$$\Gamma^{(k)}_{(ij)} = \frac{\sqrt{g_{kk}}}{\sqrt{g_{ii}}\sqrt{g_{jj}}}\Gamma^k_{ij} - \delta^k_i\frac{g_{im}}{g_{ii}\sqrt{g_{jj}}}\Gamma^m_{ij} \quad (\text{sum on } m) \tag{14}$$

δ^k_i is the Kronecker delta function. Γ^i_{jk} is the Christoffel symbol of the second kind and is defined as

$$\Gamma^i_{jk} = \frac{1}{2}g^{ip}\left[\frac{\partial g_{jp}}{\partial \xi^k} + \frac{\partial g_{kp}}{\partial \xi^j} - \frac{\partial g_{jk}}{\partial \xi^p}\right] \quad (\text{sum on } p) \tag{15}$$

Each term in Equation (1) is expressed as

$$
\begin{aligned}
(\nabla \underline{u}) \cdot \underline{u} &= u^{(k)} u^{(i)}_{(k)} \underline{a}_{(i)} \quad \text{(sum on } i \text{ and } k\text{)} \\
\nabla P &= g^{(ik)} \frac{\partial P}{\partial \xi^{(k)}} \underline{a}_{(i)} \quad \text{(sum on } i \text{ and } k\text{)} \\
\nabla^2 \underline{u} &= g^{(jk)} \left[u^{(m)}_{(j)} \Gamma^{(i)}_{(mk)} - u^{(i)}_{(m)} \Gamma^{(m)}_{(jk)} + \frac{\partial u^{(i)}_{(j)}}{\xi^{(k)}} \right] \underline{a}_{(i)} \quad \text{(sum on } i, j, k \text{ and } m\text{)}
\end{aligned}
\tag{16}
$$

$$
[\nabla \underline{u} + (\nabla \underline{u})^{\mathrm{T}}] \cdot \nabla v_E = [g^{(jk)} u^{(i)}_{(k)} + g^{(ik)} u^{(j)}_{(k)}] \frac{\partial \nabla v_E}{\partial \xi^{(j)}} \underline{a}_{(i)} \quad \text{(sum on } i, j \text{ and } k\text{)}
$$

Each physical covariant base vector $\underline{a}_{(i)}$ is independent; therefore the physical curvilinear component form of RANS equations could be expressed as Equation (4). Each term in Equation (3) is expressed as

$$
\begin{aligned}
\nabla^2 P &= -g^{(jk)} \Gamma^{(i)}_{(kj)} \frac{\partial P}{\partial \xi^{(i)}} + g^{(ij)} \frac{\partial^2 P}{\partial \xi^{(j)} \partial \xi^{(i)}} \quad \text{(sum on } i, j \text{ and } k\text{)} \\
(\nabla \underline{u})^{\mathrm{T}} : \nabla \underline{u} &= u^{(k)}_{(i)} u^{(i)}_{(k)} \quad \text{(sum on } i \text{ and } k\text{)} \\
\nabla^2 \underline{u} \cdot \nabla v_E &= g^{(jk)} \frac{\partial v_E}{\partial \xi^{(i)}} \left[u^{(m)}_{(j)} \Gamma^{(i)}_{(mk)} - u^{(i)}_{(m)} \Gamma^{(m)}_{(jk)} + \frac{\partial u^{(i)}_{(j)}}{\xi^{(k)}} \right] \\
&\quad \text{(sum on } i, j, k \text{ and } m\text{)}
\end{aligned}
\tag{17}
$$

$$
[\nabla \underline{u} + (\nabla \underline{u})^{\mathrm{T}}] : \nabla(\nabla v_E) = -[g^{(mj)} u^{(k)}_{(m)} + g^{(mk)} u^{(j)}_{(m)}] \Gamma^{(i)}_{(kj)} \frac{\partial v_E}{\partial \xi^{(i)}} + [g^{(mj)} u^{(i)}_{(m)} + g^{(im)} u^{(j)}_{(m)}] \times \frac{\partial^2 v_E}{\partial \xi^{(j)} \partial \xi^{(i)}} \quad \text{(sum on } i, j, k \text{ and } m\text{)}
$$

Equations (4)–(6) are transformed once more to make a standard form for the finite analytic method. The stretched coordinates are used to make a standard form and are defined as

$$
\triangle \xi^{i*} = \frac{1}{\sqrt{g^{ii}}} \triangle \xi^{i} \tag{18}
$$

The standard form is given by

$$
\frac{\partial^2 \phi}{\partial \xi^{1*} \partial \xi^{1*}} + \frac{\partial^2 \phi}{\partial \xi^{2*} \partial \xi^{2*}} + \frac{\partial^2 \phi}{\partial \xi^{3*} \partial \xi^{3*}} = A \frac{\partial \phi}{\partial \xi^{1*}} + B \frac{\partial \phi}{\partial \xi^{2*}} + C \frac{\partial \phi}{\partial \xi^{3*}} + D \frac{\partial \phi}{\partial \tau} + S_\phi \tag{19}
$$

The ϕ represents velocity components $u^{(1)}$, $u^{(2)}$, $u^{(3)}$, and P. Equation (19) is linearized by assuming that A, B and C are constant over the local element. The non-linearity is approximately preserved by the iteration. Equation (19) is solved at the node points with the boundary conditions specified for the local neighbouring cell faces. The finite analytic approach, based on one-dimensional finite analytic solutions, is described in the next section.

3. DISCRETIZATION METHOD

A finite analytic method was used to discretize the RANS equations, kinematic boundary condition and pressure Poisson equation. The method is based on a one-dimensional finite analytic solution in a local cell. The discretization of Equation (19) is obtained using the superposition of one-dimensional finite analytical solutions [4]. The values on the cell faces are interpolated using local analytic solution having a width of four nodal points. This scheme is capable of evaluating non-uniform grid spacings and of capturing both steady and unsteady solutions of the governing equations with finite analytic boundary conditions [5].

Equation (19) is split into four one-dimensional equations

$$\frac{\partial^2\phi}{\partial\xi^{1*}\partial\xi^{1*}} - A\frac{\partial\phi}{\partial\xi^{1*}} = G_1 \tag{20}$$

$$\frac{\partial^2\phi}{\partial\xi^{2*}\partial\xi^{2*}} - B\frac{\partial\phi}{\partial\xi^{2*}} = G_2 \tag{21}$$

$$\frac{\partial^2\phi}{\partial\xi^{3*}\partial\xi^{3*}} - C\frac{\partial\phi}{\partial\xi^{3*}} = G_3 \tag{22}$$

$$-D\frac{\partial\phi}{\partial\tau} = G_4 \tag{23}$$

where

$$G_1 = -\frac{\partial^2\phi}{\partial\xi^{2*}\partial\xi^{2*}} - \frac{\partial^2\phi}{\partial\xi^{3*}\partial\xi^{3*}} + B\frac{\partial\phi}{\partial\xi^{2*}} + C\frac{\partial\phi}{\partial\xi^{3*}} + D\frac{\partial\phi}{\partial\tau} + S_\phi$$

$$G_2 = -\frac{\partial^2\phi}{\partial\xi^{1*}\partial\xi^{1*}} - \frac{\partial^2\phi}{\partial\xi^{3*}\partial\xi^{3*}} + A\frac{\partial\phi}{\partial\xi^{1*}} + C\frac{\partial\phi}{\partial\xi^{3*}} + D\frac{\partial\phi}{\partial\tau} + S_\phi$$

$$G_3 = -\frac{\partial^2\phi}{\partial\xi^{1*}\partial\xi^{1*}} - \frac{\partial^2\phi}{\partial\xi^{2*}\partial\xi^{2*}} + A\frac{\partial\phi}{\partial\xi^{1*}} + B\frac{\partial\phi}{\partial\xi^{2*}} + D\frac{\partial\phi}{\partial\tau} + S_\phi$$

$$G_4 = -\frac{\partial^2\phi}{\partial\xi^{1*}\partial\xi^{1*}} - \frac{\partial^2\phi}{\partial\xi^{2*}\partial\xi^{2*}} - \frac{\partial^2\phi}{\partial\xi^{3*}\partial\xi^{3*}} + A\frac{\partial\phi}{\partial\xi^{1*}} + B\frac{\partial\phi}{\partial\xi^{2*}} + C\frac{\partial\phi}{\partial\xi^{3*}} + S_\phi$$

Equations (20)–(22) are elliptic PDEs, whereas Equation (23) is a hyperbolic PDE. The source terms S_ϕ, G_1, G_2, G_3, and G_4 are assumed to be constant in a local cell. The length of the local elements is defined as

$$h = \Delta\xi^{1*} = \frac{1}{\sqrt{g^{11}}}, \quad k = \Delta\xi^{2*} = \frac{1}{\sqrt{g^{22}}}, \quad l = \Delta\xi^{3*} = \frac{1}{\sqrt{g^{33}}} \tag{24}$$

The one-dimensional finite analytic solution in each coordinate direction is obtained by specifying the boundary condition at the boundaries of the local element and fixing the other coordinate directions and time. For example, the analytic solution for the one-dimensional

equation in Equation (20) can be defined as

$$\phi(\xi^{1*}) = a(e^{A\xi^{1*}} - 1) + b\xi^{1*} - \frac{S_1}{A} \tag{25}$$

The coefficients a and b are determined by applying the boundary condition at two end-cell faces. The finite analytic solutions for the one-dimensional equations (20) and (23) are obtained as

$$\phi_P = a_d\phi_d + a_u\phi_u - C_{px}G_1 \tag{26}$$

$$\phi_P = a_n\phi_n + a_s\phi_s - C_{py}G_2 \tag{27}$$

$$\phi_P = a_e\phi_e + a_w\phi_w - C_{pz}G_3 \tag{28}$$

$$\phi_P = a_t\phi_t + a_b\phi_b - C_{pt}G_4 \tag{29}$$

where

$$a_d = \frac{1 - e^{-Ah_U/2}}{e^{Ah_D/2} - e^{-Ah_U/2}} \quad a_u = \frac{e^{Ah_D/2} - 1}{e^{Ah_D/2} - e^{-Ah_U/2}} \quad C_{px} = \frac{1}{2A}\frac{h_D(e^{-Ah_U/2} - 1) + h_U(e^{Ah_D/2} - 1)}{e^{Ah_D/2} - e^{-Ah_U/2}}$$

$$a_n = \frac{1 - e^{-Bh_S/2}}{e^{Bh_N/2} - e^{-Bh_S/2}} \quad a_s = \frac{e^{Bh_N/2} - 1}{e^{Bh_N/2} - e^{-Bh_S/2}} \quad C_{py} = \frac{1}{2B}\frac{h_N(e^{-Bh_S/2} - 1) + h_S(e^{Bh_N/2} - 1)}{e^{Bh_N/2} - e^{-Bh_S/2}}$$

$$a_e = \frac{1 - e^{-Ch_W/2}}{e^{Ch_E/2} - e^{-Ch_W/2}} \quad a_w = \frac{e^{Ch_E/2} - 1}{e^{Ch_E/2} - e^{-Ch_W/2}} \quad C_{pz} = \frac{1}{2C}\frac{h_E(e^{-Ch_W/2} - 1) + h_W(e^{Ch_E/2} - 1)}{e^{Ch_E/2} - e^{-Ch_W/2}}$$

$$a_t = 0 \quad a_b = 1 \quad C_{pt} = \frac{\triangle t}{2D}$$

In Equation (26), the subscripts u and d denote the upstream and the downstream nodal faces in the ξ^{1*} coordinate direction. The value at point p is obtained from the values at the u and d cell faces. The finite analytic solution for the other equations can be obtained similarly. The finite analytic coefficients in Equation (29) are approximated by assuming sufficiently large positive value of D. The following relationship can be obtained by adding each equation in Equations (20)–(23).

$$G_1 + G_2 + G_3 + G_4 = S_\phi \tag{30}$$

Finally, the finite analytic scheme based on one-dimensional finite analytic solutions is obtained by substituting the equations for G_1, G_2, G_3 and G_4 in Equations (26)–(29) into Equation (30) as

$$a_p\phi_P = \frac{1}{C_{px}}[a_d\phi_d + a_u\phi_u] + \frac{1}{C_{py}}[a_n\phi_n + a_s\phi_s] + \frac{1}{C_{pz}}[a_e\phi_e + a_w\phi_w] + \frac{1}{C_{pt}}[a_t\phi_t + a_b\phi_b] - S_\phi \tag{31}$$

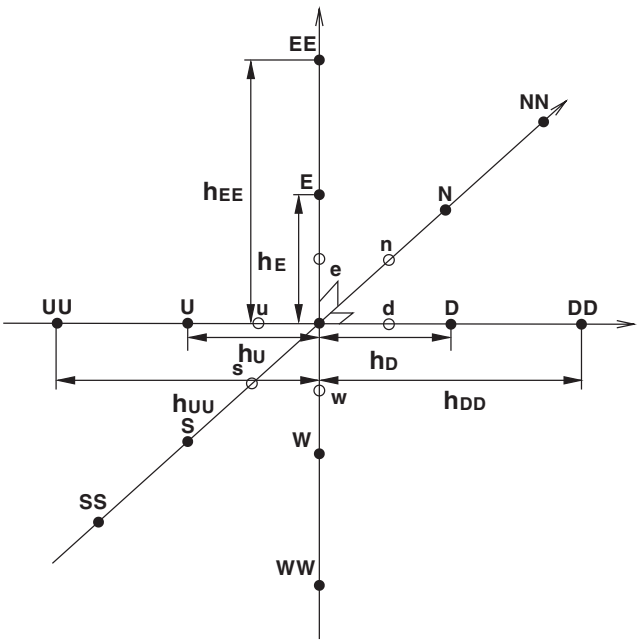

Figure 1. Local element.

where

$$a_p = \left[\frac{1}{C_{pt}} + \frac{1}{C_{px}} + \frac{1}{C_{py}} + \frac{1}{C_{pz}} \right]$$

In order to obtain more highly accurate solutions, dependent variables on the cell faces are interpolated by applying a one-dimensional analytic solution. The value on cell face u, in Figure 1 can be solved analytically for a local cell by applying the boundary conditions at points U and D, or at points UU and U. Here, the value on cell face u, obtained by applying the boundary condition at points U and D, was different from the value obtained by applying the boundary condition at points UU and U. Therefore, in this work, the value ϕ on the cell face is defined by averaging the two as [5]

$$\begin{aligned} \phi_d &= \frac{\phi_d^+ + \phi_d^-}{2}, \quad \phi_u = \frac{\phi_u^+ + \phi_u^-}{2}, \quad \phi_n = \frac{\phi_n^+ + \phi_n^-}{2}, \quad \phi_s = \frac{\phi_s^+ + \phi_s^-}{2} \\ \phi_e &= \frac{\phi_e^+ + \phi_e^-}{2}, \quad \phi_w = \frac{\phi_w^+ + \phi_w^-}{2}, \quad \phi_b = \frac{\phi_b^+ + \phi_b^-}{2} \end{aligned} \tag{32}$$

ϕ_u^+ is defined by applying the boundary condition at points UU and U to Equation (25) while ϕ_u^- is defined by applying the boundary condition at points U and D to Equation (25) as

$$\phi_u^+ = C_{UU1}^+ \phi_{UU} + C_{U1}^+ \phi_U + C_{P1}^+ \phi_P \tag{33}$$

$$\phi_u^- = C_{U1}^- \phi_U + C_{P1}^- \phi_P + C_{D1}^- \phi_D \tag{34}$$

Similarly, ϕ_d^+ and ϕ_d^+ are defined as

$$\phi_d^+ = C_{U2}^+ \phi_U + C_{P2}^+ \phi_P + C_{D2}^+ \phi_D \tag{35}$$

$$\phi_d^- = C_{P2}^- \phi_P + C_{D2}^- \phi_D + C_{DD2}^- \phi_{DD} \tag{36}$$

Therefore, ϕ_u and ϕ_d on the cell face are expressed using Equation (32) as

$$\begin{aligned} \phi_u &= \frac{C_{UU1}^+}{2}\,\phi_{UU} + \frac{C_{U1}^+ + C_{U1}^-}{2}\,\phi_U + \frac{C_{P1}^+ + C_{P1}^-}{2}\,\phi_P + \frac{C_{D1}^-}{2}\,\phi_D \\ \phi_d &= \frac{C_{U2}^+}{2}\,\phi_U + \frac{C_{P2}^+ + C_{P2}^-}{2}\,\phi_P + \frac{C_{D2}^+ + C_{D2}^-}{2}\,\phi_D + \frac{C_{DD2}^-}{2}\,\phi_{DD} \end{aligned} \tag{37}$$

where

$$C_{UU1}^+ = \frac{-h_U e^{-Ah_U/2} + \frac{h_U}{2}\,e^{-Ah_U} + \frac{h_U}{2}}{h_{UU}e^{-Ah_U} - h_U e^{-Ah_{UU}} - (h_{UU} - h_U)} \quad C_{U1}^+ = \frac{h_{UU}e^{-Ah_U/2} + \frac{h_U}{2}\,e^{-Ah_{UU}} - \left(h_{UU} - \frac{h_U}{2}\right)}{h_{UU}e^{-Ah_U} - h_U e^{-Ah_{UU}} - (h_{UU} - h_U)}$$

$$C_{D1}^- = \frac{h_U e^{-Ah_U/2} - \frac{h_u}{2}\,e^{-Ah_U} - \frac{h_U}{2}}{h_U e^{Ah_D} + h_D e^{-Ah_U} - (h_U + h_D)} \quad C_{U1}^- = \frac{h_D e^{-Ah_U/2} + \frac{h_U}{2}\,e^{Ah_D} - \left(h_D + \frac{h_U}{2}\,h_u\right)}{h_U e^{Ah_D} + h_D e^{-Ah_U} - (h_U + h_D)}$$

$$C_{P1}^+ = 1 - (C_{UU1}^+ + C_{U1}^+) \quad \text{and} \quad C_{P1}^- = 1 - (C_{U1}^- + C_{D1}^-)$$

$$C_{U2}^+ = \frac{h_D e^{Ah_D/2} - \frac{h_D}{2}\,e^{Ah_D} - \frac{h_D}{2}}{h_D e^{-Ah_U} + h_U e^{Ah_D} - (h_U + h_D)} \quad C_{D2}^+ = \frac{h_U e^{Ah_D/2} + \frac{h_D}{2}\,e^{-Ah_U} - \left(h_U + \frac{h_D}{2}\right)}{h_D e^{-Ah_U} + h_U e^{Ah_D} - (h_U + h_D)}$$

$$C_{D2}^- = \frac{h_{DD}e^{Ah_D/2} - \frac{h_D}{2}\,e^{Ah_{DD}} - \left(h_{DD} - \frac{h_D}{2}\right)}{h_{DD}e^{Ah_D} - h_D e^{Ah_{DD}} - (h_{DD} - h_D)} \quad C_{DD2}^- = \frac{-h_D e^{Ah_D/2} + \frac{h_D}{2}e^{Ah_D} + \frac{h_D}{2}}{h_{DD}e^{Ah_D} - h_D e^{Ah_{DD}} - (h_{DD} - h_D)}$$

$$C_{P2}^+ = 1 - (C_{D2}^+ + C_{U2}^+) \quad \text{and} \quad C_{P2}^- = 1 - (C_{DD2}^- + C_{D2}^-)$$

The values ϕ_n, ϕ_s, ϕ_e, and ϕ_w at the other cell faces can be obtained in the same manner. ϕ_b^+ and ϕ_b^- in Equation (32) is defined as

$$\phi_b^+ = C_{BB1}^+ \phi_{BB} + C_{B1}^+ \phi_B + C_{P1}^+ \phi_P \quad \text{where } C_{BB1}^+ = -\tfrac{1}{2}\ C_{B1}^+ = \tfrac{3}{2}\ C_{P1} = 0 \tag{38}$$

$$\phi_b^- = C_{B1}^- \phi_B + C_{P1}^- \phi_P + C_{T1}^- \phi_T \quad \text{where } C_{B1}^- = \tfrac{1}{2}\ C_{P1}^- = \tfrac{1}{2}\ C_{T1} = 0 \tag{39}$$

Here, $\phi_{BB} = \phi_P^{n-1}$, $\phi_B = \phi_P^n$, and $\phi_P = \phi_P^{n+1}$. The analytic coefficients in Equations (38) and (39) are approximated by assuming sufficiently large positive values of D. ϕ_b on the

cell face is expressed as

$$\phi_b = -\tfrac{1}{4}\phi_P^{n-1} + \phi_P\phi_P^n + \tfrac{1}{4}\phi_P^{n+1} \tag{40}$$

4. FORMULATION OF BOUNDARY CONDITIONS

When simulating free surface flow around a ship hull, the computational domain is finite and boundary conditions must be imposed at the boundaries. Then the flow field is solved numerically in the finite domain. To accurately solve this problem, appropriate boundary conditions must be imposed. To preserve higher-order accuracy at the boundaries of the computational domain, finite analytic boundary conditions for the present higher-order finite analytic schemes are formulated for inflow, outflow, impermeable surfaces and the symmetry surface. The basic principle underlying the derivation of finite analytic boundary conditions is to use the discretized form of the governing equations. On boundaries where viscous effects can be considered to be negligible, the fluid is assumed to be inviscid. In this case, the governing equations become hyperbolic differential equations

$$-A\frac{\partial\phi}{\partial\xi^{1*}} = G_1 \quad \text{where } G_1 = B\frac{\partial\phi}{\partial\xi^{2*}} + C\frac{\partial\phi}{\partial\xi^{3*}} + D\frac{\partial\phi}{\partial\tau} + S_\phi \tag{41}$$

$$-B\frac{\partial\phi}{\partial\xi^{2*}} = G_2 \quad \text{where } G_2 = A\frac{\partial\phi}{\partial\xi^{1*}} + C\frac{\partial\phi}{\partial\xi^{3*}} + D\frac{\partial\phi}{\partial\tau} + S_\phi \tag{42}$$

$$-C\frac{\partial\phi}{\partial\xi^{3*}} = G_3 \quad \text{where } G_3 = A\frac{\partial\phi}{\partial\xi^{1*}} + B\frac{\partial\phi}{\partial\xi^{2*}} + D\frac{\partial\phi}{\partial\tau} + S_\phi \tag{43}$$

The second derivative terms are added to the left-hand side of the above equations to make the standard form of the finite analytic method. Then, to minimize the effects of the second derivative terms, they can be multiplied by very small values. Then, the finite analytic solution for the one-dimensional hyperbolic PDE can be solved in a similar manner (see Section 3). The finite analytic coefficients are approximated according to the signs of A, B, and C:

$$\text{If } A > 0, \quad a_d = 0,\ a_u = 1,\ C_{px} = h_U/2A \quad \text{else } a_d = 1,\ a_u = 0,\ C_{px} = -h_D/2A$$

$$\text{If } B > 0, \quad a_n = 0,\ a_s = 1,\ C_{py} = h_S/2B \quad \text{else } a_n = 1,\ a_s = 0,\ C_{py} = -h_N/2B$$

$$\text{If } C > 0, \quad a_e = 0,\ a_w = 1,\ C_{pz} = h_W/2C \quad \text{else } a_e = 1,\ a_w = 0,\ C_{pz} = -h_E/2C$$

Also, the analytic coefficients at each cell face in Equation (37) are approximated as

$$\text{If } A>0, \quad C^+_{UU1} = -\frac{h_U}{2(h_{UU}-h_U)}, \quad C^+_{U1} = 1 + \frac{(h_U)}{2(h_{UU}-h_U)}, \quad C^-_{U1} = 0.5, \quad C^-_{D1} = 0$$

$$C^+_{U2} = -\frac{h_D}{2h_U}, \quad C^+_{P2} = 1 + \frac{(h_D)}{2h_U}, \quad C^-_{D2} = 0.5, \quad C^-_{DD2} = 0$$

$$\text{else } C^+_{UU1}=0, \quad C^+_{U1}=0.5, \quad C^-_{U1}=1+\frac{h_U}{2h_D}, \quad C^-_{D1}=-\frac{h_U}{2h_D}$$

$$C^+_{U2}=0, \quad C^+_{D2}=0.5, \quad C^-_{D2}=1+\frac{h_D}{2(h_{DD}-h_D)}, \quad C^-_{DD2}=-\frac{h_D}{2(h_{DD}-h_D)}$$

ϕ_n, ϕ_s, ϕ_e, and ϕ_w, on the cell faces can be expressed similarly. The boundary conditions are applied to the cell faces but not at the nodes. The present finite analytic boundary condition can be applied to both elliptic and hyperbolic PDEs.

4.1. At $i=2$ or $j=2$ or $k=2$ plane

Inflow, wall and symmetry conditions are given at $i=2$, $j=2$ and $k=2$ planes, respectively. The boundary conditions on these planes depend on the signs of A, B, and C. On inflow, viscous effects are negligible and the boundary equations can be considered inviscid. The values of the cell faces in Equation (31) must be specified for co-directional and contra-directional inflows. The finite analytic coefficients in Equation (31) and the velocity components at the cell faces can then be approximated. The inflow boundary conditions depend on the sign of A as

$$\text{If } A>0, \quad a_d=0, \quad a_u=1, \quad C_{px}=\frac{h_U}{2A}$$

$$\phi_u=\phi^-_u=C^-_{U1}\phi_U+C^-_{P1}\phi_P+C^-_{D1}\phi_D \quad \text{where } C_{U1}=0.5 \quad C_{P1}=0.5 \quad C_{D1}=0$$

$$\text{else } a_d=1, \quad a_u=0, \quad C_{px}=-\frac{h_D}{2A}$$

$$\phi_d=\frac{\phi^+_d+\phi^-_d}{2}=\frac{C^+_{U2}}{2}\phi_U+\frac{C^+_{P2}+C^-_{P2}}{2}\phi_P+\frac{C^+_{D2}+C^-_{D2}}{2}\phi_D+\frac{C^-_{DD2}}{2}\phi_{DD}$$

$$\frac{C^+_{U2}}{2}=0 \quad \frac{C^+_{P2}+C^-_{P2}}{2}=\frac{1}{4} \quad \frac{C^+_{D2}+C^-_{D2}}{2}=\frac{3}{4}+\frac{h_D}{4(h_{DD}-h_D)} \quad \frac{C^-_{DD2}}{2}=-\frac{h_D}{4(h_{DD}-h_D)}$$

When A is negative, no boundary condition is required because $a_u=0$ in Equation (31) and $C^+_{U2}=0$ in Equation (37). When A is positive, however, a boundary condition must be applied. Here, we assume that $\phi_u=\phi^-_u$ and $\phi_U=\phi_P$ because the values of ϕ_{UU} and ϕ_U are unknown. Therefore, we set $\phi_u=\phi_U$ when A is positive. In summary, the boundary condition on inflow is as follows:

$$\text{If } A>0, \quad \phi_u=\phi_U \quad \text{else No boundary condition is needed}$$

The above boundary conditions can be applied to velocity components and wave height. However, the boundary conditions for the pressure are different; it is assumed that there is a zero gradient.

Along the wall boundary, the components of velocity are known and a zero gradient is applied to the pressure. Viscous effects are considered at this boundary. The boundary conditions at impermeable surfaces depend on the sign of B as follows:

$$\text{If } B>0, \ \phi_s=\phi_S \quad \text{else } \phi_s=\phi^-_s=C^-_{S1}\phi_S+C^-_{P1}\phi_P+C^-_{N1}\phi_N$$

We assume that $\phi_s = \phi_s^-$. Therefore, an approximate condition was used at solid wall boundaries.

On the symmetry plane, the values of ϕ_{WW} and ϕ_W are known from the symmetry conditions. Figure 1 shows the positions of W and WW. The boundary condition at the symmetry plane depends on the sign of C

$$\text{If } C > 0, \quad a_e = 0, \quad a_w = 1, \quad C_{pz} = \frac{h_W}{2C}$$

$$\phi_w = \frac{\phi_w^+ + \phi_w^-}{2} = \frac{C_{WW1}^+}{2}\phi_{WW} + \frac{C_{W1}^+ + C_{W1}^-}{2}\phi_W + \frac{C_{P1}^+ + C_{P1}^-}{2}\phi_P + \frac{C_{E1}^-}{2}\phi_E$$

$$\text{else } a_e = 1, \quad a_w = 0, \quad C_{pz} = -\frac{h_E}{2C}$$

$$\phi_e = \frac{\phi_e^+ + \phi_e^-}{2} = \frac{C_{W2}^+}{2}\phi_W + \frac{C_{P2}^+ + C_{P2}^-}{2}\phi_P + \frac{C_{E2}^+ + C_{E2}^-}{2}\phi_E + \frac{C_{EE2}^-}{2}\phi_{EE}$$

For any sign of C, no boundary condition is required.

4.2. *At* $i = ni - 1$ *or* $j = nj - 1$ *or* $k = nk - 1$ *plane*

Exit, lateral and upper boundary conditions are given at $i = ni - 1$, $j = nj - 1$ and $k = nk - 1$ planes, respectively. To accurately solve the free surface problem, one must impose appropriate boundary conditions on these boundaries that allow waves to pass freely without spurious reflections through them. The effects of wave reflections at open boundaries can seriously degrade the accuracy of the computations, and may render the computational solution entirely unacceptable. However, this is not a simple problem to overcome. For outflow, boundary conditions are applied at cell faces in Equation (31). Viscosity effects can be considered negligible. The boundary conditions for the velocity components and wave height at the exit plane depend on the sign of A as:

$$\text{If } A > 0, \quad a_d = 0, \quad a_u = 1, \quad C_{px} = \frac{h_S}{2A}$$

$$\phi_u = \frac{\phi_u^+ + \phi_u^-}{2} = \frac{C_{UU1}^+}{2}\phi_{UU} + \frac{C_{U1}^+ + C_{U1}^-}{2}\phi_U + \frac{C_{P1}^+ + C_{P1}^-}{2}\phi_P + \frac{C_{D1}^-}{2}\phi_D$$

$$\frac{C_{UU1}^+}{2} = -\frac{h_U}{4(h_{UU} - h_U)} \quad \frac{C_{U1}^+ + C_{U1}^-}{2} = \frac{3}{4} + \frac{h_U}{4(h_{UU} - h_U)} \quad \frac{C_{P1}^+ + C_{P1}^-}{2} = \frac{1}{4}\quad \frac{C_{D1}^-}{2} = 0$$

$$\text{else } a_d = 1, \quad a_u = 0, \quad C_{px} = -\frac{h_N}{2A}$$

$$\phi_d = \phi_d^+ = C_{U2}^+\phi_U + C_{P2}^+\phi_P + C_{D2}^+\phi_D \quad \text{where } C_{U2}^+ = 0 \quad C_{P2}^+ = 0.5 \quad C_{D2}^+ = 0.5$$

When A is positive, no boundary condition is required because $a_d = 0$ in Equation (31) and $C_{D1}^- = 0$ in Equation (37). However, an appropriate boundary condition is required for a negative A. Here, we assume that $\phi_d = \phi_d^+$ and $\phi_D = \phi_P$ because the values of ϕ_{DD} and ϕ_D

are unknown, therefore we set $\phi_d = \phi_P$. However, boundary conditions may yield small reflections for the negative sign at open boundaries because of the above assumption. For the pressure, a zero gradient is applied. After all assumptions have been incorporated, the boundary condition at the exit plane is as follows:

$$\text{If } A > 0 \text{ No boundary condition is needed} \quad \text{else } \phi_d = \phi_P$$

The same boundary condition can be applied to other planes similarly.

5. LOWER-ORDER BOUNDARY CONDITION

The finite analytic boundary conditions suggested in the present work is based on higher-order accuracy. The boundary conditions are used at the cell faces on the boundaries. When the comparative method is used, another type of boundary condition can be considered, which can be applied directly at the nodes. Thus, Dirichlet and Neumann boundary conditions can be applied on the boundaries. However, the boundary conditions are based on lower-order accuracy and the accuracy can suffer near the boundaries.

Coefficients a and b in Equations (25) are determined by applying the boundary condition at the two end node points. The finite analytic solution for the one-dimensional equations in Equations (26)–(28) is rewritten as

$$\phi_P = a_D \phi_D + a_U \phi_U - C_{PX} G_1 \tag{44}$$

$$\phi_P = a_N \phi_N + a_S \phi_S - C_{PY} G_2 \tag{45}$$

$$\phi_P = a_E \phi_E + a_W \phi_W - C_{PZ} G_3 \tag{46}$$

where

$$a_D = \frac{1 - e^{-Ah_U}}{e^{Ah_D} - e^{-Ah_U}} \quad a_U = \frac{e^{Ah_D} - 1}{e^{Ah_D} - e^{-Ah_U}} \quad C_{PX} = \frac{1}{A} \frac{h_D(e^{-Ah_U} - 1) + h_U(e^{Ah_D} - 1)}{e^{Ah_D} - e^{-Ah_U}}$$

$$a_N = \frac{1 - e^{-Bh_S}}{e^{Bh_N} - e^{-Bh_S}} \quad a_S = \frac{e^{Bh_N} - 1}{e^{Bh_N} - e^{-Bh_S}} \quad C_{PY} = \frac{1}{B} \frac{h_N(e^{-Bh_S} - 1) + h_S(e^{Bh_N} - 1)}{e^{Bh_N} - e^{-Bh_S}}$$

$$a_E = \frac{1 - e^{-Ch_W}}{e^{Ch_E} - e^{-Ch_W}} \quad a_W = \frac{e^{Ch_E} - 1}{e^{Ch_E} - e^{-Ch_W}} \quad C_{PZ} = \frac{1}{C} \frac{h_E(e^{-Ch_W} - 1) + h_W(e^{Ch_E} - 1)}{e^{Ch_E} - e^{-Ch_W}}$$

The finite analytic coefficients on the boundaries where viscous effects can be negligible, are approximated as

$$\text{If } A > 0, \quad a_D = 0,\ a_U = 1,\ C_{PX} = h_U/A \quad \text{else } a_D = 1,\ a_U = 0,\ C_{PX} = -h_D/A$$

$$\text{If } B > 0, \quad a_N = 0,\ a_S = 1,\ C_{PY} = h_S/B \quad \text{else } a_N = 1,\ a_S = 0,\ C_{PY} = -h_N/B$$

$$\text{If } C > 0, \quad a_E = 0,\ a_W = 1,\ C_{PZ} = h_W/C \quad \text{else } a_E = 1,\ a_W = 0,\ C_{PZ} = -h_E/C$$

Equations (44)–(46) are used only on the boundary in each direction. Namely, on inflow and outflow, the discretized form is expressed as

$$a_p\phi_P = \frac{1}{C_{PX}}[a_D\phi_D + a_U\phi_U] + \frac{1}{C_{py}}[a_n\phi_n + a_s\phi_s] + \frac{1}{C_{pz}}[a_e\phi_e + a_w\phi_w]$$
$$+\frac{1}{C_{pt}}[a_t\phi_t + a_b\phi_b] - S_\phi$$

At impermeable surface and lateral boundary plane, the discretized form is expressed as

$$a_p\phi_P = \frac{1}{C_{px}}[a_d\phi_d + a_u\phi_u] + \frac{1}{C_{PY}}[a_N\phi_N + a_S\phi_S] + \frac{1}{C_{pz}}[a_e\phi_e + a_w\phi_w]$$
$$+\frac{1}{C_{pt}}[a_t\phi_t + a_b\phi_b] - S_\phi$$

It is not necessary to interpolate dependent values at the cell faces. The discretized form at other boundaries can be expressed similarly.

6. COMPUTATION

The pressure Poisson equation method and the kinematic boundary conditions are used to solve the velocity–pressure–wave height coupling problem for the incompressible RANS equations. The matrix, which consists of the coefficients resulting from the finite analytic method, is solved using the generalized minimal residual (GMRES) method [21] to enhance the convergence rate of RANS equations, the kinematic boundary condition and the pressure Poisson equation. An interface-tracking method is used to define the free surface as a sharp interface. The meshes are fitted to the interface at each time step, and no interface smearing takes place. Its upper boundary always coincides with the boundaries of the fluid flow. The kinematic condition is solved by using the momentum equations in a coupled manner and is itself used to update the unknown location of the free surface. An unsteady structured grid generation solver is used in this work [4]. The Baldwin–Lomax model was used with the wall function to calculate the eddy viscosity in the turbulent flow [22, 23].

The Wigley hull was used as a ship model. The simulation was performed for the hull advancing in calm water. The example shown here is for the free-surface waves around a Wigley hull. This is an example of an open boundary problem with far field boundaries. The equation for the hull geometry is given by

$$z = \frac{B}{2}\left[1 - \left(\frac{2x}{L}\right)^2\right]\left[1 - \left(\frac{y}{D}\right)^2\right]$$

where B is the breadth, L is the length, and D is the draft of the ship. The computational domain is one length on the side and one length below the ship hull. The upstream and downstream boundaries were placed at a distance far away from the hull, $x/L = -3$ and 6, respectively. The boundary condition for P in Equation (1) on inflow is set to zero. Also,

turbulence kinetic energy, k is set to zero; therefore, the pressure in this plane is $-z/Fn^2$. For the computation of turbulent flow, the spacing off the body is very small, so the simple Neumann condition is applied for the pressure. The wave generated in the interior of the computational domain propagates to the open boundaries and leaves these boundaries. On the open boundary, the non-reflecting boundary condition should be applied to pass the wave through the open boundary.

The three-dimensional free-moving turbulent flow was computed. The upper boundary moves arbitrarily with the flow, and the grid in the computational domain is generated every time step until the steady state solution is obtained. Only two iterations for each time step were used for computing the higher order effect of all equations. No acceleration of the flow was used to reach the final speed. All computations were performed by an implicit method without adding any artificial dissipative terms. The computations were performed without a relaxation factor. The time increment of 0.005 was used for two different Froude numbers, 0.267 and 0.289. The Reynolds number used in the computation was 3.3×10^6. All computations were executed with a grid size of $127 \times 45 \times 35$. All computations were performed for 1200 time steps of 6 s each. However, the converged state near the hull surface was reached within a mere 400 time steps. Convergent steady-state results for the Wigley hull were compared with experiment data and the data were taken from References [24–26]. The simulations are performed to demonstrate the validity of the present higher-order finite analytic scheme. Two different boundary conditions are applied on the boundaries for each simulation. The calculated results are compared with available experimental data at two Froude numbers, 0.267 and 0.289. Figures 2 and 3 show a comparison of free surface profiles on the hull surface. The two different boundary conditions, lower-order and higher-order, were compared. In Figure 2, a deviation of wave profiles between experiments and computations was observed in the bow region. The bow peak is not captured properly. A deviation in the bow waves is also found at $Fn = 0.289$. The higher-order boundary condition was used at the cell faces on the boundaries, while the lower-order condition was applied at the nodes. The higher-order condition does not seem to give a more accurate prediction of the free surface profiles on the hull surface than the lower-order condition. Figures 4 and 5 show wave elevation contours at $Fn = 0.267$ in the upper boundary of the Wigley hull at two different time steps. Due to the approximations assumed at open boundaries, small reflections were created, but were not serious and could reasonably be ignored. The two different boundary conditions were compared. The divergent and the transverse waves are observed. The simulations model the near-field waves accurately. However, there is a glaring discrepancy in the far field at $y/L > 0.2$ off the hull surface. The influence of the higher-order effects is found in the far field; specifically, the far field waves are underpredicted by the simulation that uses the lower-order boundary condition. The improvement achieved by the present scheme was obtained in far field by using higher-order finite analytic boundary condition. Experimental data are available for $Fn = 0.267$. This gives a perspective view of the free surface waves. Figure 6 shows a comparison of wave elevation contours at $t = 6$ s with experimental data. The higher-order boundary condition could be applied to improve the accuracy of the solution for the far field waves. Figure 7 shows a comparison of wave elevation contours at another Fn. The grid and the computational domain are the same as those for $Fn = 0.267$. The improvement in far field is also found. The far field waves may differ due to the effects of the grid size and the grid density. For the same size and density of a grid, however, it can be concluded that the improvement in far field waves is due to the higher-order at the boundaries. Therefore, some improvement on the

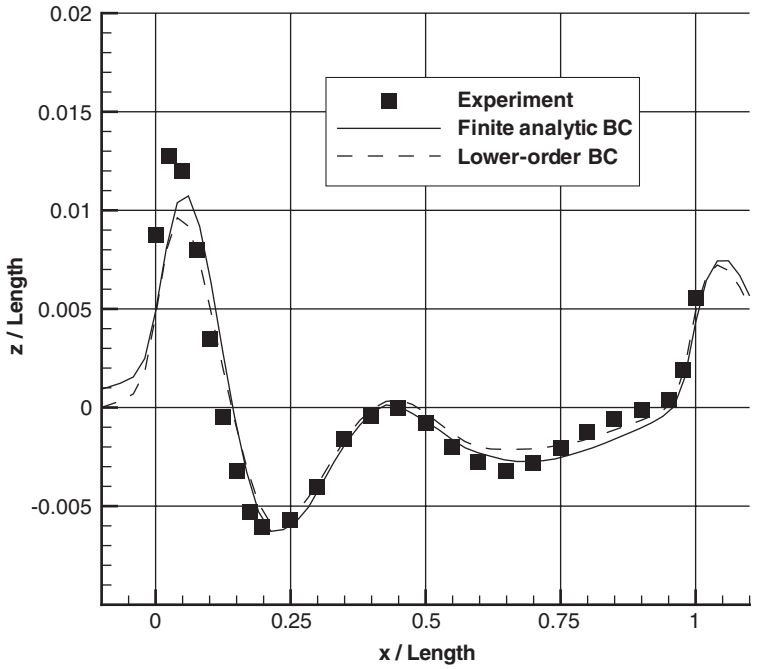

Figure 2. Comparison of free surface profiles on hull surface at $Fn = 0.267$.

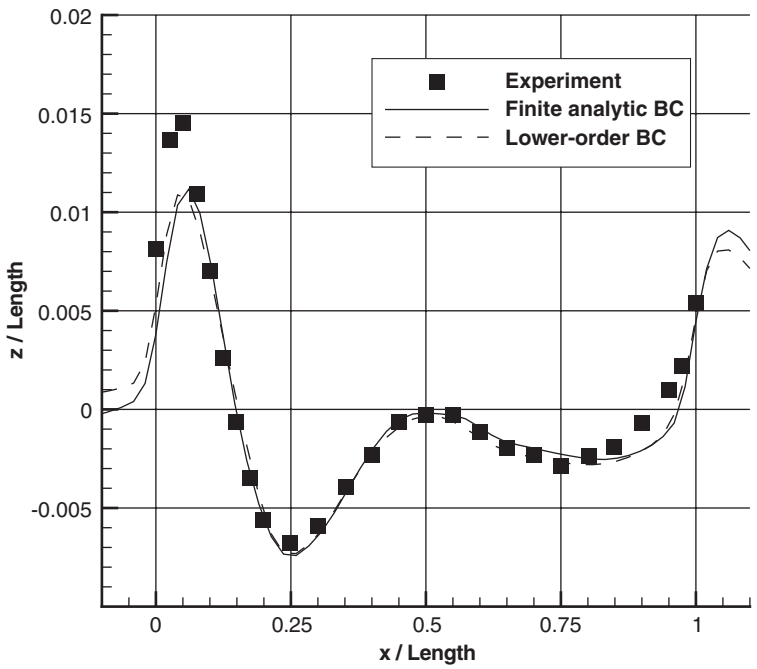

Figure 3. Comparison of free surface profiles on hull surface at $Fn = 0.289$.

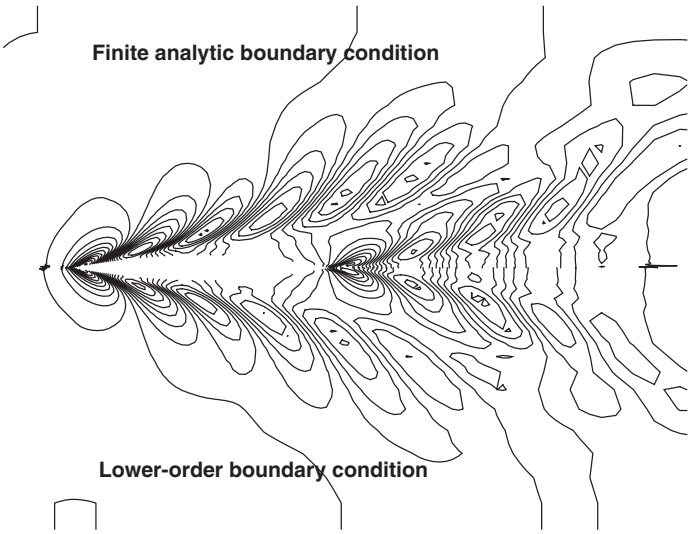

Figure 4. Comparison of wave elevation contours at $t = 2$ and $Fn = 0.267$.

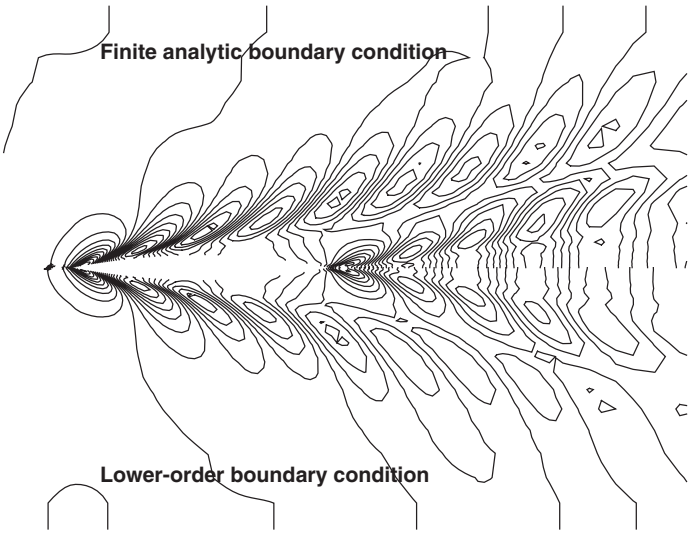

Figure 5. Comparison of wave elevation contours at $t = 4$ and $Fn = 0.267$.

waves could be achieved with the higher-order boundary condition. It was shown that more computational time steps were needed to get a sufficiently accurate free surface prediction at distances far away from the hull.

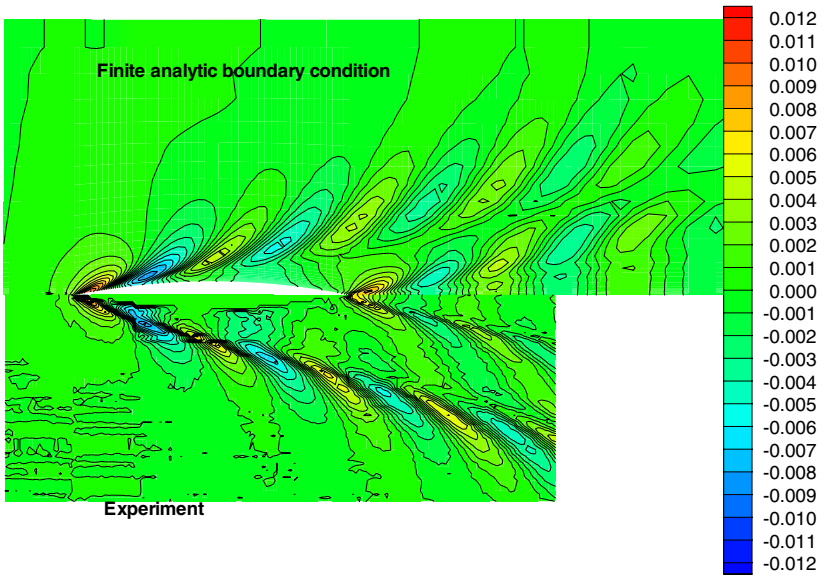

Figure 6. Comparison of wave elevation contours at $t = 6$ and $Fn = 0.267$.

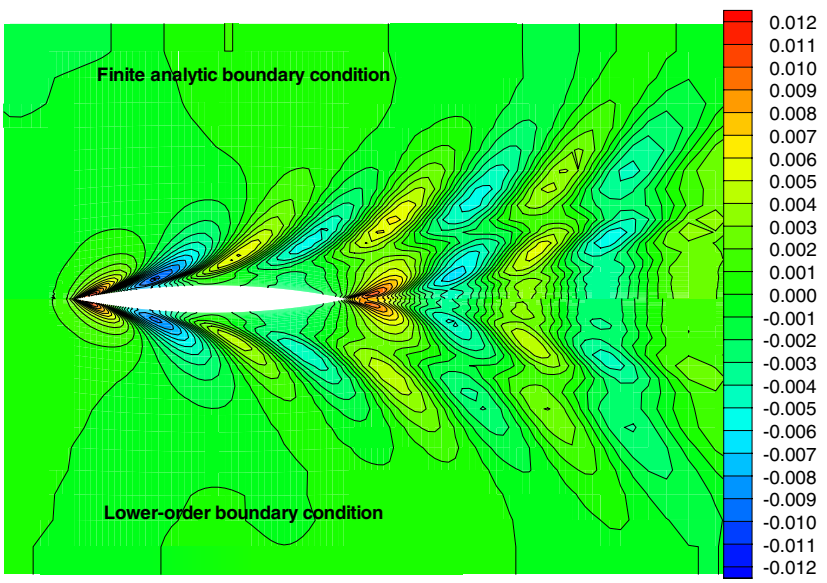

Figure 7. Comparison of wave elevation contours at $t = 6$ and $Fn = 0.289$.

7. SUMMARY

A novel approach to numerically simulate incompressible free surface flows based on physical curvilinear coordinate system was investigated. A higher order finite analytic scheme based on a one-dimensional analytic solution was applied to the discretization of the incompressible RANS equations, the kinematic boundary condition and the pressure Poisson equation. Finite analytic boundary conditions based on higher-order schemes were proposed for inflow, outflow, symmetry plane and impermeable surfaces. At the boundaries, two different finite analytic boundary conditions have been suggested. One is lower-order and the other is higher-order. The numerical results for the computations of free surface flow around a Wigley hull demonstrated here indicated that the present numerical scheme and boundary conditions were adapted to three-dimensional incompressible free surface flow. Two different finite analytic boundary conditions were compared through the computations of the free surface flow. This comparison demonstrated that the use of the higher-order boundary condition was necessary to achieve a sufficiently accurate far field prediction. It was shown that a new numerical scheme and new boundary conditions could be used to solve three-dimensional elliptic and hyperbolic PDEs.

ACKNOWLEDGEMENTS

The experimental data were provided by the Department of Systems Design for Ocean-Space, Yokohama National University. The Authors wish to particularly thank Dr Kazuo Suzuki.

REFERENCES

1. Chen CJ, Chen HC. Finite analytic method. *IIHR Report No. 232-IV*, The University of Iowa, 1982.
2. Chen HC, Patel VC, Ju S. Solutions of Reynolds-averaged Navier–Stokes equations for three-dimensional incompressible flows. *Journal of Computational Physics* 1990; **88**:305–336.
3. Chen CJ, Bravo RH, Chen HC, Xu Z. Accurate discretization of incompressible three-dimensional Navier–Stokes equations. *Numerical Heat Transfer*, *Part B* 1995; **27**:371–392.
4. Lee SH, Soni BK. The enhancement of an elliptic grid using appropriate control functions. *Applied Mathematics and Computation* 2004; **159**:809–821.
5. Ohring S. Three-dimensional ship wave generation using an efficient finite difference scheme with double model linearization. *Journal of Computational Physics* 1981; **41**:89–114.
6. Hino T. Computation of a free surface flow around an advancing ship by the Navier–Stokes equations. *4th International Conference on Numerical Ship Hydrodynamics*, Japan, 1989.
7. Miyata H, Sata T, Baba N. Difference solution of a viscous flow with free-surface wave about an advancing ship. *Journal of Computational Physics* 1987; **72**:393–421.
8. Tahara Y, Stern F. A large-domain approach for calculating ship boundary layers and Wakes fields for nonzero Froude number. *Journal of Computational Physics* 1996; **127**:398–411.
9. Beddhu M, Jiang MY, Taylor LK, Whitfield DL. Computation of steady and unsteady flows with a free surface around the Wigley hull. *Applied Mathematics and Computation* 1998; **89**:67–84.
10. Farmer J, Martinelli L, Jameson A. Fast multigrid method for solving incompressible hydrodynamic problems with free surface. *AIAA Journal* 1994; **32**:1175–1182.
11. Li T. Computation of turbulent free-surface flows around modern ships. *International Journal for Numerical Methods in Fluids* 2003; **43**:407–430.
12. Guillerm PE, Alessandrini B. 3D Free-surface flow computation using a RABSE/Fourier–Kochin coupling. *International Journal for Numerical Methods in Fluids* 2003; **43**:301–318.
13. Alessandrini B, Delhommeau G. A fully coupled Navier–Stokes solver for calculation of turbulent incompressible free surface flow past a ship hull. *International Journal for Numerical Methods in Fluids* 1999; **29**:125–142.
14. Zhao C, Liu T. Non-reflecting artificial boundaries for transient scalar wave propagation in a two-dimensional infinite homogenous layer. *International Journal for Numerical Methods in Fluids* 2003; **58**:1435–1456.
15. Joolen VJV, Neta B, Givoli D. Higher-order boundary conditions for linearized shallow water equations with stratification, dispersion and advection. *International Journal for Numerical Methods in Fluids* 2004; **46**:361–381.

16. Krenk S. Unified formulation of radiation condition for the wave equation. *International Journal for Numerical Methods in Fluids* 2002; **53**:275–295.
17. Huan R, Thompson LL. Accurate radiation boundary conditions for the time-dependent wave equation on unbounded domains. *International Journal for Numerical Methods in Fluids* 2000; **47**:1569–1603.
18. Ol'shanskii MA, Staroverov VM. On simulation of outflow boundary conditions in finite difference calculations for incompressible fluid. *International Journal for Numerical Methods in Fluids* 2000; **33**:499–534.
19. Harlow F, Welch J. Numerical calculation of time-dependent viscous incompressible flow of fluid with free surfaces. *Physics of Fluids* 1965; **8**:2181–2189.
20. Lee SH. Three-dimensional incompressible viscous solutions based on the physical curvilinear coordinate system. *Ph.D. Dissertation*, Department of Computational Engineering, Mississippi State University, 1997.
21. Saad T, Schultz MH. GMRES: a generalized minimal residual algorithm for solving non-symmetric linear systems. *SIAM Journal on Scientific and Statistical Computing* 1986; **7**:856–869.
22. Baldwin BS, Lomax H. Thin layer approximation and algebraic model for separated turbulent flows. *AIAA Paper 78-257*, 1978.
23. Launder BE, Spalding DB. The numerical computation of turbulent flows. *Computer Methods in Applied Mechanics and Engineering* 1974; **3**:269–289.
24. ITTC. Cooperative experiments on Wigley parabolic models in Japan. *17th ITTC Resistance Committee Report*, 1984.
25. Ikehata M, Katou M, Yanagita F. Automation of wave height measurement around a model. *Transactions of the West-Japan Society of Naval Architects* 1998; **95**:57–66.
26. Farmer J. A finite volume multigrid solution to the three dimensional nonlinear ship wave problem. *Ph.D. Thesis*, Department of Mechanical and Aerospace Engineering, Princeton University, 1993.

